

## Exchange energies in CoFeB/Ru/CoFeB synthetic antiferromagnets

A. Mouhoub<sup>1,\*</sup>, F. Millo<sup>1</sup>, C. Chappert<sup>1</sup>, J.-V. Kim<sup>1</sup>, J. Létang<sup>1</sup>, A. Solignac<sup>2</sup>, and T. Devolder<sup>1</sup><sup>1</sup>Université Paris-Saclay, CNRS, Centre de Nanosciences et de Nanotechnologies, 91120 Palaiseau, France<sup>2</sup>SPEC, CEA, CNRS, Université Paris-Saclay, 91191 Gif-sur-Yvette, France

(Received 4 November 2022; accepted 13 March 2023; published 10 April 2023)

The interlayer exchange coupling confers specific properties to synthetic antiferromagnets that make them suitable for several applications of spintronics. The efficient use of this magnetic configuration requires an in-depth understanding of the magnetic properties and their correlation with the material structure. Here we establish a reliable procedure to quantify the interlayer exchange coupling and the intralayer exchange stiffness in synthetic antiferromagnets; we apply it to the ultrasmooth and amorphous  $\text{Co}_{40}\text{Fe}_{40}\text{B}_{20}$  (5–40 nm)/Ru/ $\text{Co}_{40}\text{Fe}_{40}\text{B}_{20}$  material platform. The complex interplay between the two exchange interactions results in a gradient of the magnetization orientation across the thickness of the stack which alters the hysteresis and the spin wave eigenmodes of the stack in a nontrivial way. We measured the field dependence of the frequencies of the first four spin waves confined within the thickness of the stack. We modeled these frequencies and the corresponding thickness profiles of these spin waves using micromagnetic simulations. The comparison with the experimental results allows us to deduce the magnetic parameters that best account for the sample behavior. The exchange stiffness is established to be  $16 \pm 2$  pJ/m, independent of the  $\text{Co}_{40}\text{Fe}_{40}\text{B}_{20}$  thickness. The interlayer exchange coupling starts from  $-1.7$  mJ/m<sup>2</sup> for the thinnest layers, and it can be maintained above  $-1.3$  mJ/m<sup>2</sup> for CoFeB layers as thick as 40 nm. The comparison of our method with earlier characterizations using the sole saturation fields argues for a need to revisit the tabulated values of interlayer exchange coupling in thick synthetic antiferromagnets.

DOI: [10.1103/PhysRevMaterials.7.044404](https://doi.org/10.1103/PhysRevMaterials.7.044404)

## I. INTRODUCTION

Synthetic antiferromagnets (SAFs) are a class of artificial multilayers consisting of two identical ferromagnetic layers separated by a nonmagnetic spacer that favors antiparallel magnetizations thanks to an interlayer coupling [1]. This interlayer coupling is an additional degree of freedom that confers a large tunability to SAFs and allows the customization of their magnetic properties for specific applications. As stray-field-free magnets, SAFs triggered, for instance, interest as part of stable reference layers in sensors or as free layers in random access memory applications [2,3]. SAFs have also been used in high-performance spin-torque oscillators [4] or as a medium in which domain walls can reach exceptionally high velocities [5]. Recently, SAFs entered the field of magnonics [6], where the remarkable anisotropy and nonreciprocity of their spin waves (SWs) have attracted attention [7,8].

It is therefore important to develop methods to properly measure the magnetic properties of SAFs and to understand their correlation with the material structure of the multilayer stack. The two layers of the SAF are coupled by two distinct phenomena: the (electron-mediated) interlayer exchange interaction [9] and the (roughness-mediated) so-called “Néel” dipolar coupling [10,11]. Their sum is described by an interfacial energy  $J_{\text{tot}} = J_{\text{Néel}} + J_{\text{ex}}$  or an equivalent field  $H_J = -\frac{2J_{\text{tot}}}{\mu_0 M_s t_{\text{mag}}}$ , where  $M_s$  is the saturation magnetization and

$t_{\text{mag}}$  is the thickness of each of the (identical) layers of the SAF;  $J$  is conventionally deduced by confusing  $H_J$  with the saturation field, i.e., the field that sets the two magnets of the SAF in a parallel state along the easiest direction [12–15]. However, this approach is inaccurate when the magnetizations of the two layers are not strictly uniform across their thickness. This happens as soon as  $t_{\text{mag}}$  becomes comparable or larger than one of the two characteristic lengths of the system: the bulk exchange length [16]  $\lambda_B = \sqrt{2A_{\text{ex}}/(\mu_0 M_s^2)}$ , where  $A_{\text{ex}}$  is the bulk (intralayer) exchange stiffness, and the depth  $\lambda_I = A_{\text{ex}}/J_{\text{tot}}$  in which the magnetization orientation in the bulk of a sample feels the micromagnetic state at the two interfaces of the interlayer spacer.

In many of the currently used SAFs, the condition  $t_{\text{mag}} \ll \{\lambda_I, \lambda_B\}$  is not fulfilled; we will, for instance, conclude that  $\lambda_I \approx 10$  nm and  $\lambda_B \approx 4$  nm in our SAFs. So when a field is applied, the magnetizations in the regions far from the spacer reorient, while those close to the interfaces with the spacer keep their magnetizations more antiparallel. The magnetic hysteresis and the spin waves are considerably modified by this gradient of the magnetization orientation. In this case,  $J$  cannot be evaluated from the sole knowledge of the saturation field: A more elaborate method taking into account the competition between inter- and intralayer exchange must be developed.

Here we study the material structure, the magnetic hysteresis, the spin wave frequencies, and the spin wave thickness profile in a series of SAFs with relevant thicknesses spanning from near  $\lambda_I$  and  $\lambda_B$  to much thicker. By fitting the field dependence of the spin wave mode frequencies with

\*asma.mouhoub@u-psud.fr

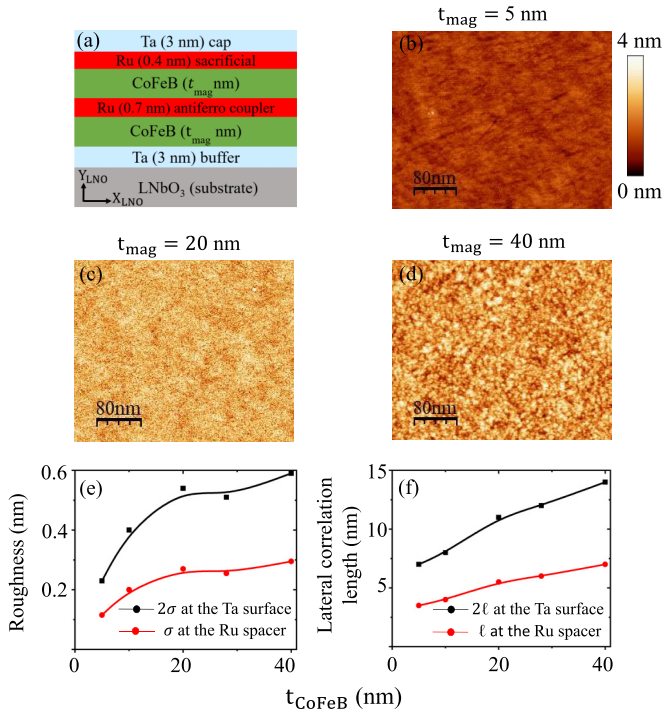


FIG. 1. Structural properties of the synthetic antiferromagnets. (a) Sketch of the nominal stack with the crystalline directions of the substrate. (b)–(d) Atomic force microscopy measurement of the surface topography ( $1 \times 1 \mu\text{m}^2$ ) of the SAFs with  $t_{\text{mag}} = 5, 20, 40$  nm. (e) Surface roughness of the SAF measured at the Ta surface ( $2\sigma$ ) and interpolated at the Ru spacer ( $\sigma$ ). (f) Lateral correlation length of the surface roughness measured at the Ta outer surface ( $2\ell$ ) and interpolated at the buried Ru spacer ( $\ell$ ).

thickness-resolved micromagnetic simulations, we deduce the intralayer exchange interaction and interlayer coupling constants with quantifiable reliability. After correction from roughness effects, we observe that a strong interlayer exchange (electron mediated) [17] interaction with  $|J_{\text{ex}}| > 1.3$  mJ/m<sup>2</sup> is maintained on structurally smooth SAFs for CoFeB layers as thick as 40 nm; this comes despite an apparently easy and very gradual saturation that arises from the gradient of the magnetization orientation which develops within the thickness of the stack.

## II. SAMPLES AND METHODS

### A. Thin film growth and structure

We grow our SAF multilayers by sputter deposition on Y-cut LiNbO<sub>3</sub> (LNO) single-crystal substrates in a chamber of base pressure below  $10^{-7}$  mbar. The deposition was conducted under an (optimized) argon pressure of  $5 \times 10^{-3}$  mbar, i.e., sufficiently low to maximize the magnetization [18]. The SAFs are symmetric with nominal composition LNO/Ta (6 nm)/Co<sub>40</sub>Fe<sub>40</sub>B<sub>20</sub> ( $t_{\text{mag}}$ )/Ru ( $t_{\text{Ru}} = 7$  Å)/Co<sub>40</sub>Fe<sub>40</sub>B<sub>20</sub> ( $t_{\text{mag}}$ )/Ru (0.4 nm)/Ta (6 nm, cap); see Fig. 1(a). The investigated CoFeB thicknesses  $t_{\text{mag}}$  are 5, 10, 15, 16.9, 20, 28, and 40 nm. The thickness of the Ru spacer was optimized to maximize the interlayer exchange coupling for our composition of CoFeB, in agreement with Ref. [19].

The Ru (0.4 nm) layer is a sacrificial layer that conveniently avoids [20] the resputtering of the top CoFeB layer when the heavy and energetic Ta atoms of the cap impinge on the stack being grown. Note that the biquadratic interlayer exchange coupling is known to be negligible for this  $t_{\text{Ru}}$  and our CoFeB composition ratio [21]. The samples are in the as-grown state;  $\theta - 2\theta$  x-ray diffraction scans (not shown) argue for a bcc (011) and (112) texture of the Ta buffer layer and an amorphous state of the CoFeB layers, as anticipated for our boron content [22].

Additional samples containing a single CoFeB layer with a thickness of 17 nm were grown for the optimization of the deposition conditions. Vibrating sample magnetometry (VSM) and vector network analyzer ferromagnetic resonance (VNA-FMR [23]) indicated that these reference samples have a saturation magnetization  $\mu_0 M_s = 1.7$  T and a damping  $\alpha = 0.0045 \pm 0.0005$ . A tiny uniaxial anisotropy (an approximate field of 3 mT) was evidenced in the film plane; we will neglect it in the following.

Our present aim is to measure the interlayer exchange coupling [17]. This requires us to correct for the other source of interlayer coupling: the roughness-induced “orange-peel” coupling [10] that opposes the exchange coupling. The orange-peel coupling depends on the standard deviation  $\sigma_{\text{rms}}$  and the lateral wavelength  $\ell$  of the conformal roughness of the Ru layer separating the two magnets [11]. The values of  $\ell$  and  $\sigma_{\text{rms}}$  at the buried Ru spacer layer are unfortunately not measurable by atomic force microscopy; however, they can be estimated from the interpolation of their values at the surface of the sample. Atomic force microscopy [Figs. 1(b) and 1(d)] indicates indeed that both the surface roughness and the lateral correlation length (the typical “grain size” at the top of the Ta cap layer) are quasilinear functions of  $t_{\text{mag}}$ : Thicker films have wider and taller grains (Fig. 1). We will thus assume that the values of  $\ell$  and  $\sigma_{\text{rms}}$  at the Ru spacer layer are the halves of their (measured) value at the surface. The structure is clearly grainy [see, e.g., Fig. 1(d)]; however, the autocorrelation function of the surface height measured by atomic force microscopy has a single maximum (its  $\delta$  correlation): It does not show any secondary peak that would indicate the existence of a most probable grain size from which an unquestionable value of  $\ell$  could be given. We shall thus consider that the lateral wavelength  $\ell$  of the roughness can be approximated by the full width at half maximum (FWHM) of this height autocorrelation function. Note that a potential error in  $\ell$  does not induce a large error in the Néel coupling since  $J_{\text{Néel}}$  is only weakly dependent on  $\ell$  when  $\ell \gg t_{\text{Ru}}$ . Indeed, following Ref. [11], the orange-peel coupling energy is

$$J_{\text{Néel}} = 2\sqrt{2}\pi^2 \frac{(\sigma_{\text{rms}})^2}{\ell} \mu_0 M_s^2 \exp\left(-2\pi\sqrt{2}\frac{t_{\text{Ru}}}{\ell}\right), \quad (1)$$

which can be evaluated using the topographical data of Figs. 1(e) and 1(f). Note that the above equation assumes a one-dimensional periodic roughness [10], which in principle cannot be applied to any topography with a broad two-dimensional distribution of the in-plane periods  $\ell$ . Equation (1) can, however, be reliably used because its variation is dominated by that of  $\sigma_{\text{rms}}$ . The orange-peel coupling is negligible for our thinnest layers, but it should rise to

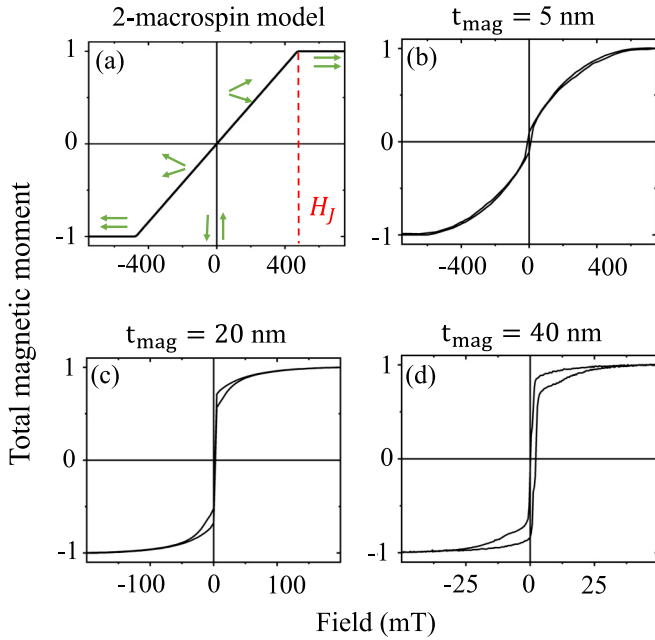


FIG. 2. Quasistatic magnetic properties of the synthetic anti-ferromagnets. (a) Simulated hysteresis loop of the two-macrospin model. (b)–(d) Experimental hysteresis loops of the SAFs for  $t_{\text{mag}} = 5, 20, 40$  nm.

$+0.33 \pm 0.02$  mJ/m<sup>2</sup> for  $t_{\text{mag}} \geq 20$  nm when a grainy topography becomes perceivable [see Fig. 1(c)]. These values and their uncertainty will be used to identify the pure exchange part in the *total* interlayer coupling energies that we will determine in Sec. III.

## B. Magnetic measurements

### 1. Magnetic hysteresis

The hysteresis loops of the films measured by VSM are reported in Figs. 2(b)–2(d). They will be fitted to their theoretical counterparts obtained from exact micromagnetic simulations (Fig. 4); however, for a start it is convenient to compare them to a toy model in which two identical macrospins (labeled 1 and 2) are coupled through a total interlayer coupling  $J_{\text{tot}} = J_{\text{ex}} + J_{\text{Néel}}$ . In this two-macrospin description the loop is linear [Fig. 2(a)], i.e.,  $\frac{M_x}{M_s} = \frac{H_x}{H_{J,\text{tot}}}$  until a clear saturation for  $|H_x| \geq H_{J,\text{tot}}$ : The antiparallel (AP) remanent state evolves to the saturated (parallel) state through a gradual scissoring of the macrospins [see sketches in Fig. 2(a)].

While very thin SAFs can have quasilinear hysteresis loops resembling the two-macrospin approximation (see, for instance, Refs. [14,24]), the loop of our thinnest SAF sample ( $t_{\text{mag}} = 5$  nm) already shows a clear rounding [Fig. 2(b)]. The saturation in thicker SAFs requires smaller fields [Figs. 2(c) and 2(d)], reflecting the thickness dependence of the exchange field. Unfortunately, the rounding of the loop becomes too pronounced to define a saturation field in the presence of experimental noise. This rounding will be discussed later together with the dynamical properties of the SAFs. A slight opening of the hysteresis loop is present in the thickest films

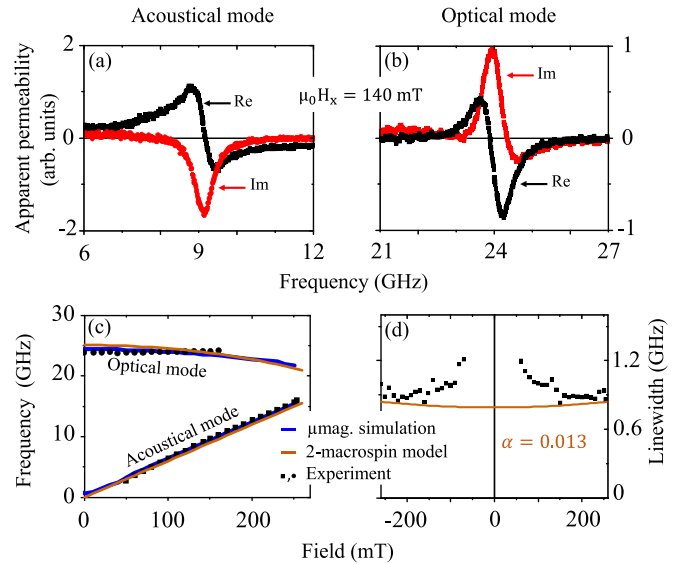


FIG. 3. Dynamic magnetic properties of a SAF with  $t_{\text{mag}} = 5$  nm. Apparent permeability for an applied field of 140 mT in frequency windows around the acoustical (a) and optical (b) spin wave modes. (c) Field dependence of the mode frequencies, compared with the two-macrospin model and with the micromagnetic ( $\mu\text{mag.}$ ) model with a thickness stratification  $n_z = 16$ . The models are evaluated with  $M_s = 1.35 \times 10^6$  A/m,  $J_{\text{tot}} = -1.64$  mJ/m<sup>2</sup>, and  $A_{\text{ex}} = 16$  pJ/m. (d) Field dependence of the linewidth (FWHM) of the acoustical mode, and comparison with the Gilbert linewidth  $\frac{\Delta\omega_{\text{ac}}}{2\pi} = \frac{\alpha\gamma_0}{2\pi} \left( M_s + \frac{H_j^2 + H_x^2}{H_j} \right)$  for a damping of  $\alpha = 0.013$ .

[Fig. 2(d)]; there the structural defects (e.g., the grainy structure) and the small but nonvanishing anisotropy probably lead to some irreversibility in the magnetization process.

### 2. Spin waves

The frequencies  $f_{j,\text{exp}}$  of the spin waves (SWs) of the samples were identified using vector network analyzer ferromagnetic resonance (VNA-FMR [23]) in in-plane applied fields up to  $\mu_0 H_x = 250$  mT. In this method, the SAF is inductively coupled to a microwave coplanar waveguide. The frequency dependence of the impedance of this ensemble is used to extract the transverse susceptibility spectrum of the sample. Figures 3(a) and 3(b) display representative spectra for both the acoustical and optical spin wave modes [25] of the stack. Owing to the metallic nature of the SAF, the electromagnetic fields of the coplanar waveguide are shielded in a frequency-dependent manner [26], such that the apparent susceptibility can be rotated in the complex plane. To correct this, the spin wave modes are simply identified as maxima in the modulus of the apparent susceptibility, and the linewidth of each mode is set by a generalized Lorentzian fit. For the thinnest SAFs,  $t_{\text{mag}} \leq 20$  nm, only two spin wave modes could be detected (see the example in Fig. 3 for  $t_{\text{mag}} = 5$  nm and in the Supplemental Material [27]). Four SW modes were detected for the thicker SAFs as will be further discussed in Fig. 5(a).

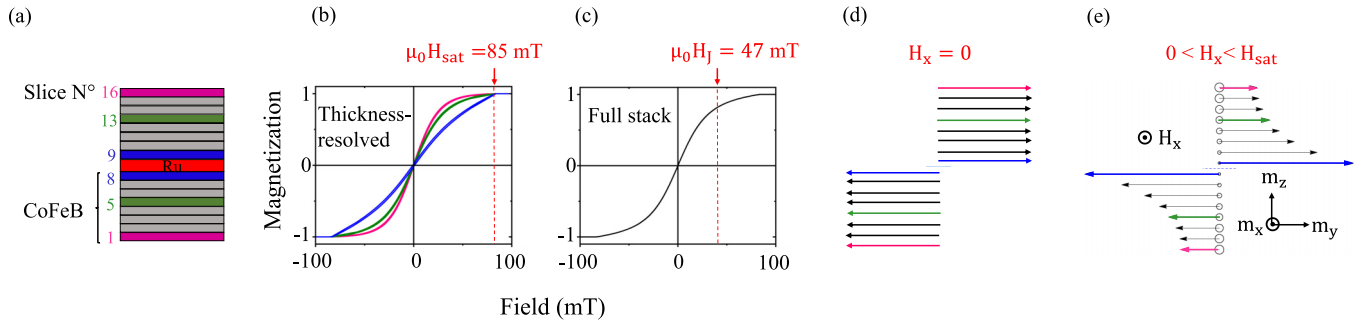


FIG. 4. Thickness-resolved hysteresis loop of a SAF with  $t_{\text{mag}} = 40$  nm from micromagnetic simulations. (a) Sketch of the chosen stratification of the CoFeB layers. (b) Selected slice-resolved hysteresis loops and (c) total moment of the stack. (d) and (e) Sketch of the gradient of magnetization orientation along  $z$  at remanence and at finite applied field. (b) and (c) are evaluated for  $t_{\text{mag}} = 40$  nm,  $M_s = 1.35 \times 10^6$  A/m,  $J_{\text{tot}} = J_{\text{ex}} = -1$  mJ/m<sup>2</sup>, and  $A_{\text{ex}} = 16$  pJ/m. The arrows in (b) and (c) recall the values of the saturation field  $H_{\text{sat}}$  and the interlayer exchange field  $H_J$ .

### C. Magnetic models

#### 1. Spin waves in the two-macrospin model

For an approximate description of the thinnest SAFs we first stick to the two-macrospin model. For  $0 \leq H_x < H_{J,\text{tot}}$  the system is in the scissor state and possesses two excitation modes: the acoustical and optical spin wave modes of frequencies [28]  $\frac{\omega_{\text{ac}}}{2\pi} = \frac{\gamma_0}{2\pi} H_x \sqrt{\frac{M_s + H_{J,\text{tot}}}{H_{J,\text{tot}}}}$  and  $\frac{\omega_{\text{op}}}{2\pi} = \frac{\gamma_0}{2\pi} \sqrt{\frac{M_s}{H_{J,\text{tot}}}} \sqrt{H_{J,\text{tot}}^2 - H_x^2}$ , where  $\gamma_0$  is the gyromagnetic ratio. This simplified description seems still valid for our thinnest SAF with  $t_{\text{mag}} = 5$  nm, as plotted in Fig. 3(c).

For thicker SAFs, the magnetizations within the thickness of each CoFeB layer can twist at a moderate exchange energy cost. In this case we need a full micromagnetic description, for which we use the software MUMAX3 [29].

#### 2. Hysteresis in the micromagnetic description

In our micromagnetic simulations, the material is described with a saturation magnetization  $\mu_0 M_s = 1.7$  T and a damping  $\alpha = 0.0045$ . The simulated shape is a cuboid of

dimensions  $\{320 \text{ nm} \times 320 \text{ nm} \times 2t_{\text{mag}}\}$ . Periodic boundary conditions are set in the sample plane (i.e.,  $xy$ ) to mimic an infinite thin film. The sample is meshed into  $128 \times 128 \times n_z$  cells. The stratification  $n_z = 16$  is chosen in the thickness direction to have cells thinner than  $\lambda_B$  even for our thickest SAFs. We disregard the spacer thickness and implement a direct interlayer coupling between the two magnetic layers of the SAF, i.e., at the frontier between the slices  $i = 8$  and 9. For each applied field  $H_x$ , we let the system relax to its ground state, allowing us to plot either the hysteresis loop of the total moment  $\frac{1}{n_z} \sum_{i=1}^{n_z} \frac{M_x^i}{M_s}$  versus the applied field  $H_x$  [Fig. 4(c)], or the hysteresis loop of a specific slice  $M_x^i/M_s$ . Figure 4(b) shows, for instance, the loop of the Ru-facing slice ( $i = 8$ , blue) and the top slice ( $i = 1$  or 16, magenta). The corresponding gradient of the magnetization orientation across the thickness is sketched in Fig. 4(e).

#### 3. Micromagnetic determination of the spin waves

We now aim to study the laterally uniform spin waves (SWs) of the system in a thickness-resolved manner. To

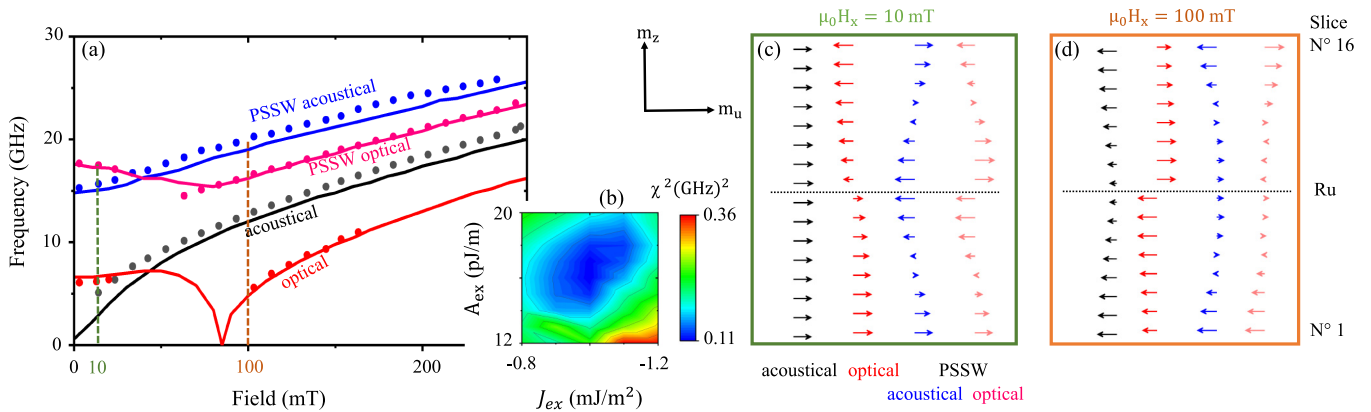


FIG. 5. Spin waves of a SAF with  $t_{\text{mag}} = 40$  nm. (a) Experimental frequencies of the spin wave modes (symbols) vs micromagnetic modeling (solid lines). (b) Map of the distance  $\chi_{\text{fit}}^2$  between the experimental set of SW frequencies and the model in the  $\{A_{\text{ex}}, J_{\text{tot}}\}$  plane. (c) Simulated thickness profiles of the dynamic magnetic components for the four spin wave modes at an applied field of  $\mu_0 H_x = 10$  mT. The dynamical components are plotted in the plane transverse to the magnetization ground state. (d) The same but at a larger applied field of  $\mu_0 H_x = 100$  mT. The micromagnetic modeling is implemented with  $t_{\text{mag}} = 40$  nm,  $M_s = 1.35 \times 10^6$  A/m,  $J_{\text{tot}} = J_{\text{ex}} = -1$  mJ/m<sup>2</sup>, and  $A_{\text{ex}} = 16$  pJ/m.

TABLE I. Micromagnetic parameters that best describe the spin wave frequencies and linewidth of the  $\text{Co}_{40}\text{Fe}_{40}\text{B}_{20}/\text{Ru}$  (7 Å)/ $\text{Co}_{40}\text{Fe}_{40}\text{B}_{20}$  synthetic antiferromagnets.

Sample $t_{\text{mag}}$ (nm)	Exchange stiffness $A_{\text{ex}}$ (pJ/m)	Interlayer coupling $J_{\text{ex}} + J_{\text{Néel}}$ (mJ/m <sup>2</sup> )	Exchange part $J_{\text{ex}}$ (mJ/m <sup>2</sup> )
5	Unmeasurable	$-1.64 \pm 0.14$	$-1.68 \pm 0.16$
10	$13.4 \pm 5$	$-1.71 \pm 0.15$	$-1.85 \pm 0.19$
15	$16.2 \pm 2.9$	$-1.7 \pm 0.1$	$-1.9^{\text{a}}$
17	$16.2 \pm 3.3$	$-1.71 \pm 0.1$	$-1.94^{\text{a}}$
20	$14.8 \pm 1.6$	$-1.51 \pm 0.1$	$-1.78 \pm 0.12$
28	$16.4 \pm 1.8$	$-1.08 \pm 0.14$	$-1.33 \pm 0.15$
40	$16.4 \pm 2.5$	$-1 \pm 0.15$	$-1.33 \pm 0.17$

<sup>a</sup> $\ell$  and  $\sigma_{\text{rms}}$  were extrapolated instead of measured.

numerically excite these SWs, we let MUMAX3 calculate the slice-resolved response  $\tilde{m}_i(t)$  of the system to a laterally uniform out-of-plane field pulse superimposed on the static applied field  $H_x \vec{e}_x$ . In the slice  $i$  the pulse reads

$$\tilde{h}^{\text{pulse}}(i, t > 0) = \mathcal{H}(4 - i) \frac{\sin(\pi f_c t)}{\pi f_c t} h \vec{e}_z,$$

where  $f_c = 100$  GHz and  $h = 0.1$  mT. The Heaviside function  $\mathcal{H}$  is to apply the field pulse in the sole bottom quarter of the SAF (slices  $1 \leq i \leq 4$ ) in order to excite all modes including the ones that are nonuniform across the thickness. We let the simulation run until  $t_{\text{simu}} = 5$  ns, and we record the magnetization in each sublayer every picosecond.

We identify the SW frequencies as those at which the power spectra  $\|\tilde{M}_{i,x}(f)\|^2$  are maximal for arbitrarily chosen  $\tilde{M}(f)$  component (here  $M_x$ ) and slice. The “ $\sim$ ” symbol recalls the complex-valued nature of  $\tilde{M}$ . The frequency-domain magnetization  $\tilde{M}(f)$  is the Fourier transform of the Hann-window apodized version of  $\tilde{m}_i(t)$ :

$$\tilde{M}_i(f) = \mathcal{F} \left[ \cos \left( \frac{\pi(t - t_{\text{simu}}/2)}{t_{\text{simu}}} \right) \tilde{m}_i(t) \right]. \quad (2)$$

We restrict our analysis to the  $j = 1, \dots, 4$  lowest frequency modes. Figure 5(a) shows the field dependence of their calculated frequencies  $f_j(H_x)$  for a set of material parameters. To ease the discussion, we shall label the SW modes according to the thickness profile of their dynamic magnetization  $\text{Re}(\tilde{M}_i(f_j))$  [see Figs. 5(b) and 5(c)]. Conventionally, acoustic (optical) modes have responses that are in phase (opposite of phase) on either side of the spacer when displayed in the precession planes  $\{\tilde{M}_i \times \vec{e}_z, \vec{e}_z\}$  transverse to the ground state. Besides, the modes with amplitude nodes within the interior of each of the two magnetic layers recall the perpendicular standing spin waves (PSSWs) of single layers [30,31]. Looking at the low-field mode profiles in Fig. 5(b), we shall refer to the  $j = 1-4$  modes as the acoustical FMR, the optical FMR, the acoustical PSSW, and the optical PSSW.

#### 4. Determination of the best-fitting material parameters

We target to determine the values of  $A_{\text{ex}}$  and  $J_{\text{tot}}$  with the best possible accuracy. We thus assess the adequacy of any chosen set of material parameters by calculating the distance  $\chi_{\text{fit}}$  between the experimental SW frequencies and their

simulated counterparts. This distance is defined as

$$\chi_{\text{fit}}^2 = \frac{1}{N} \sum_{j=1}^N (f_{j(H_x), \text{exp}} - f_{j(H_x), \text{sim}})^2, \quad (3)$$

where  $N = 2$  for  $t_{\text{mag}} \leq 20$  nm (and  $N = 4$  otherwise) is the number of experimentally observed SW modes. The best-fitting values of the material parameters for each SAF are found by minimizing  $\chi_{\text{fit}}$  in the  $\{A_{\text{ex}}, J_{\text{tot}}\}$  plane, as illustrated for the SAF with  $t_{\text{mag}} = 40$  nm in Fig. 5(b). We define the uncertainty on  $\{A_{\text{ex}}, J_{\text{tot}}\}$  as the domain in which the distance  $\chi_{\text{fit}}$  stays below twice its optimal value. The optimal values and their uncertainty are reported in Table I.

### III. RESULTS

The aim of this work is to measure the interlayer and intralayer exchange energies. As a first remark, we want to emphasize that although this was often practiced in the literature, this cannot be done from the sole hysteresis loop and the two-macrospin model. Indeed as illustrated in Figs. 4(b) and 4(c) for  $t_{\text{mag}} = 40$  nm, confusing the saturation field  $\mu_0 H_{\text{sat}} = 85$  mT with the interlayer exchange field  $\mu_0 H_J = 47$  mT would lead to dramatically overestimating  $J$ . The exact same conclusion would be drawn if  $H_{\text{sat}}$  was instead determined from the softening of the optical mode [see Fig. 5(a)].

Alternatively, one could try and fit the experimental loops with the micromagnetically modeled ones, as practiced in Ref. [32]. Unfortunately, the unavoidable noise and the substrate-induced parasitic slope in the experimental loops make it difficult to determine the true saturation field, especially when a rounding is present at the saturation. Instead, the frequencies of the SAF eigenmodes can be determined with a high degree of confidence from both the experimental data and the micromagnetic simulations.

We thus deduced the micromagnetic parameters  $\{A_{\text{ex}}, J_{\text{tot}}\}$  of the SAF from the sole criterion of matching the experimental and simulated SW frequencies through a minimization of  $\chi_{\text{fit}}$ . The obtained best-fitting values  $J_{\text{tot}}$  represent the total interlayer coupling, i.e., accounting for the sum  $J_{\text{ex}} + J_{\text{Néel}}$  of the interlayer exchange term and the orange-peel term. Table I gathers the best-fitting values of  $\{A_{\text{ex}}, J_{\text{tot}}\}$  and their confidence interval. Note that the exchange stiffness could not be determined for  $t_{\text{mag}} = 5$  nm. For the thinnest films, the PSSW modes were not detected experimentally, and the frequencies

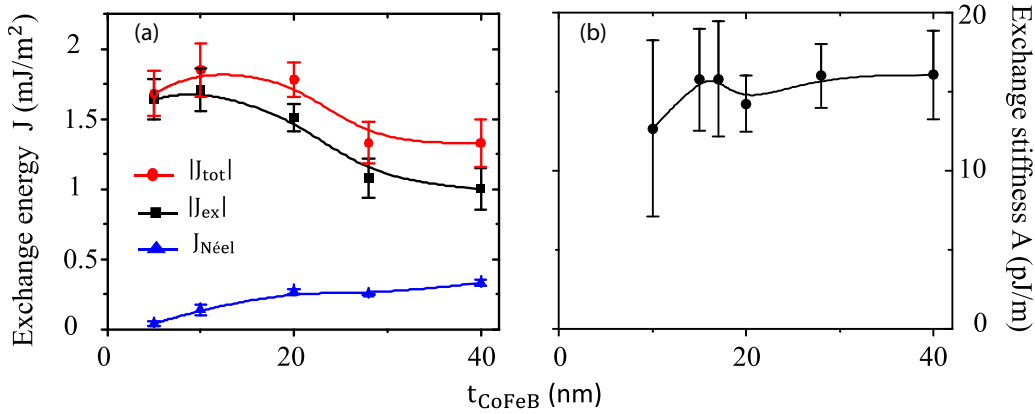


FIG. 6.  $\text{Co}_{40}\text{Fe}_{40}\text{B}_{20}$  thickness dependence of (a) the interlayer coupling energies and (b) the intralayer exchange stiffness.

of the acoustic and optical SW were almost insensitive to  $\{A_{\text{ex}}, J_{\text{tot}}\}$  in the simulations. As expected, the two-macrospin model and the micromagnetic simulations match for this specific thickness only.

We estimated the orange-peel coupling for different CoFeB thicknesses using Eq. (1). The interlayer exchange coupling in Table I is calculated by subtracting the orange-peel coupling from the total exchange. Table I indicates that the intralayer exchange stiffness of amorphous  $\text{Co}_{40}\text{Fe}_{40}\text{B}_{20}$  is  $16 \pm 2$  pJ/m and seems independent of the film thickness within our measurement accuracy (see Fig. 6). The interlayer exchange coupling is  $-1.7 \pm 0.15$  mJ/m<sup>2</sup> for the thinnest films and can be maintained above  $-1.3 \pm 0.15$  mJ/m<sup>2</sup> on structurally smooth SAFs for CoFeB layers as thick as 40 nm.

## IV. DISCUSSION

### A. Exchange stiffness

Let us first discuss the value of the exchange stiffness, found to be  $A_{\text{ex}} = 16 \pm 2$  pJ/m for our amorphous  $\text{Co}_{40}\text{Fe}_{40}\text{B}_{20}$  layers. This consolidated value is comparable to earlier reports for *amorphous* alloys of composition equal to ours: Values of 11, 13, and 14 pJ/m were found in Refs. [18,33,34], respectively. The exact value of  $A_{\text{ex}}$  was also reported to depend on the argon pressure used for the sputter deposition [18]: Values were scattered from 10 to 14 pJ/m, the latter value being obtained for an argon pressure equal to ours.

Despite this reasonable agreement with earlier reports, our number of  $16 \pm 2$  pJ/m may be regarded as surprisingly small compared with that of *crystalline* Co-Fe binary alloys such as elemental iron (20–23 pJ/m, in Refs. [35,36]), elemental cobalt (15.2, 28.5, and 30 pJ/m, in Refs. [32,34,37]),  $\text{Co}_{90}\text{Fe}_{10}$  (29.8 pJ/m in Ref. [18] and 25 pJ/m in Ref. [38]), or  $\text{Co}_{80}\text{Fe}_{20}$  (26.1 pJ/m in Ref. [39]). To understand this quantitative difference, it is worth keeping in mind that for a given composition, CoFeB alloys have substantially smaller  $A_{\text{ex}}$  when in the amorphous state as compared with when in the crystalline state [22,33]. In a comprehensive study [22], Kim *et al.* showed, for instance, that  $A_{\text{ex}}$  drops from 16 to 8 pJ/m when rendering amorphous an alloy film of approximate composition  $\text{Co}_9\text{Fe}_{86}\text{B}_5$ . Note that these values are small because

they refer to alloys on the Fe-rich side of the Co-Fe binary system.

Our conclusion that the most probable value of the exchange stiffness is  $A_{\text{ex}} = 16 \pm 2$  pJ/m for amorphous  $\text{Co}_{40}\text{Fe}_{40}\text{B}_{20}$  layers, therefore, calls for two main comments: It highlights the importance of (i) adjusting the Fe-Co composition and (ii) controlling its crystalline or amorphous state.

### B. Interlayer exchange coupling

Let us now comment on our estimate of the interlayer exchange coupling  $J_{\text{ex}} = -1.7 \pm 0.15$  mJ/m<sup>2</sup>. The comparison with the literature is more problematic as many references (e.g., Ref. [19]) either omit to report structural data (thus confusing potentially  $J_{\text{ex}}$  and  $J_{\text{tot}}$ ) and/or deduce their interlayer exchange coupling from a confusion between  $H_{\text{sat}}$  and  $H_J$ . As already highlighted in Fig. 4, the confusion between  $H_{\text{sat}}$  and  $H_J$  leads to an overestimation of  $J_{\text{ex}}$  for films thicker than  $\lambda_I$  and  $\lambda_B$ . In contrast, the confusion between  $J_{\text{ex}}$  and  $J_{\text{tot}}$  leads to an underestimation of  $J_{\text{ex}}$ , but only for nonsmooth stacks. We thus emphasize that a thorough analysis is required when looking back at literature data on the interlayer exchange coupling.

The study of Waring *et al.* [40] identified that the  $J_{\text{tot}}$  values obtained from the fitting of spin wave frequencies at remanence were smaller than the  $J_{\text{tot}}$  values obtained from the saturation field. In agreement with our conclusion in Fig. 3(a), the difference in the estimated  $J_{\text{tot}}$  is minor for their 5-nm-thick  $\text{Co}_{20}\text{Fe}_{60}\text{B}_{20}$  layers. They report a value of  $J_{\text{tot}} = -1.27$  mJ/m<sup>2</sup> after optimization of the Ru spacer thickness. Despite a different Fe-Co composition ratio, we believe that this number of  $-1.27$  mJ/m<sup>2</sup> can be compared with our  $-1.7 \pm 0.15$  mJ/m<sup>2</sup>. Indeed, Hashimoto *et al.* [21] have shown that the interlayer exchange is almost independent of the Fe-Co composition ratio in the 25%-75% and 75%-25% composition interval.

Another conclusion of our study is that contrary to earlier studies [19], the amorphous character of our magnetic films does not prevent the achievement of very strong interlayer exchange coupling, potentially as strong as in the authoritative Co/Ru (8.5 Å)/Co system, where the interlayer coupling is typically [41,42]  $J_{\text{ex}} = -1.5$  mJ/m<sup>2</sup>. The fact that  $J_{\text{ex}}$  decreases with the roughness does not change the

antiferromagnetic nature of the coupling, and this is an indication that the roughness of the spacer is conformal and that the coherence of the electron within the Ru spacer quantum well is maintained in all samples.

## V. CONCLUSION

In conclusion, we have described a procedure for the measurement of the interlayer coupling and intralayer exchange stiffness in thick and thin synthetic antiferromagnets. The procedure relies on the measurement and the modeling of the frequencies of the spin wave modes confined within the thickness of the stack, and notably their dependence with the applied field. The values of the spin wave frequencies are objective and largely immune to potential imperfections in the experimental measurements, such that the procedure yields reliable estimates of the interlayer coupling and intralayer exchange stiffness.

We have implemented our procedure on symmetric  $\text{Co}_{40}\text{Fe}_{40}\text{B}_{20}$  (5–40 nm)/Ru/ $\text{Co}_{40}\text{Fe}_{40}\text{B}_{20}$  synthetic antiferromagnets in which the magnetic layers are amorphous and of controlled roughness. The exchange stiffness is found to be  $16 \pm 2$  pJ/m, independent from the CoFeB thickness. The interlayer exchange coupling starts from  $-1.7$  mJ/m<sup>2</sup> for the thinnest layers, and it can be maintained above  $-1.3$  mJ/m<sup>2</sup>

for CoFeB layers as thick as 40 nm. Our results are compatible to the few earlier reports that carefully implemented reliable methods on comparable material systems. This comparison indicates that the amorphous character of the  $\text{Co}_{40}\text{Fe}_{40}\text{B}_{20}$  layers leads to a reduced intralayer exchange stiffness but does not seem detrimental to obtaining a large interlayer exchange coupling.

## ACKNOWLEDGMENTS

A.M. acknowledges financial support from the EOBE doctoral school of Paris-Saclay University. F.M. acknowledges the French National Research Agency (ANR) under Contract No. ANR-20-CE24-0025 (MAXSAW). J.L. acknowledges the FETOPEN-01-2016-2017 [FET-Open research and innovation actions (CHIRON project: Grant Agreement No. 801055)]. This work was also supported by a public grant overseen by the ANR as part of the Investissements d’Avenir; program (Labex NanoSaclay, Reference No. ANR-10-LABX-0035, project SPICY). We thank Sokhna-Méry Ngom, Laurent Couraud, and Ludovic Largeau for assistance in the structural characterizations. This work was done within the C2N micro nanotechnologies platforms and partly supported by the RENATECH network and the General Council of Essonne.

- 
- [1] P. Grünberg, R. Schreiber, Y. Pang, M. B. Brodsky, and H. Sowers, Layered Magnetic Structures: Evidence for Antiferromagnetic Coupling of Fe Layers across Cr Interlayers, *Phys. Rev. Lett.* **57**, 2442 (1986).
  - [2] D. C. Worledge, Spin flop switching for magnetic random access memory, *Appl. Phys. Lett.* **84**, 4559 (2004).
  - [3] J. Hayakawa, S. Ikeda, Y. M. Lee, R. Sasaki, T. Meguro, F. Matsukura, H. Takahashi, and H. Ohno, Current-induced magnetization switching in MgO barrier based magnetic tunnel junctions with CoFeB/Ru/CoFeB synthetic ferrimagnetic free layer, *Jpn. J. Appl. Phys.* **45**, L1057 (2006).
  - [4] D. Houssameddine, J. F. Sierra, D. Gusakova, B. Delaet, U. Ebels, L. D. Buda-Prejbeanu, M.-C. Cyrille, B. Dieny, B. Ocker, J. Langer, and W. Maas, Spin torque driven excitations in a synthetic antiferromagnet, *Appl. Phys. Lett.* **96**, 072511 (2010).
  - [5] S.-H. Yang, K.-S. Ryu, and S. Parkin, Domain-wall velocities of up to  $750 \text{ m s}^{-1}$  driven by exchange-coupling torque in synthetic antiferromagnets, *Nat. Nanotechnol.* **10**, 221 (2015).
  - [6] A. V. Chumak, V. I. Vasyuchka, A. A. Serga, and B. Hillebrands, Magnon spintronics, *Nat. Phys.* **11**, 453 (2015).
  - [7] A. F. Franco and P. Landeros, Enhancement of the spin-wave nonreciprocity in antiferromagnetically coupled multilayers with dipolar and interfacial Dzyaloshinskii-Moriya interactions, *Phys. Rev. B* **102**, 184424 (2020).
  - [8] R. A. Gallardo, P. Alvarado-Seguel, A. Kakay, J. Lindner, and P. Landeros, Spin-wave focusing induced by dipole-dipole interaction in synthetic antiferromagnets, *Phys. Rev. B* **104**, 174417 (2021).
  - [9] P. Bruno, Interlayer exchange coupling: a unified physical picture, *J. Magn. Magn. Mater.* **121**, 248 (1993).
  - [10] L. Néel, Sur un nouveau mode de couplage entre les aimantations de deux couches minces ferromagnétiques, *C. R. Hebd. Seances Acad. Sci.* **255**, 1676 (1962).
  - [11] B. D. Schrag, A. Anguelouch, S. Ingvarsson, G. Xiao, Y. Lu, P. L. Trouilloud, A. Gupta, R. A. Wanner, W. J. Gallagher, P. M. Rice, and S. S. P. Parkin, Néel orange-peel coupling in magnetic tunneling junction devices, *Appl. Phys. Lett.* **77**, 2373 (2000).
  - [12] F. Nguyen van Dau, A. Fert, P. Etienne, M. N. Baibich, J. M. Broto, J. Chazelas, G. Creuzet, A. Friederich, S. Hadjoudj, H. Hurdequint, J. P. Redoulès, and J. Massies, Magnetic properties of (001)Fe/(001)Cr bcc multilayers, *J. Phys. Colloq.* **49**, C8-1633 (1988).
  - [13] S. S. P. Parkin, N. More, and K. P. Roche, Oscillations in Exchange Coupling and Magnetoresistance in Metallic Superlattice Structures: Co/Ru, Co/Cr, and Fe/Cr, *Phys. Rev. Lett.* **64**, 2304 (1990).
  - [14] N. Wiese, T. Dimopoulos, M. Rühlig, J. Wecker, H. Brückl, and G. Reiss, Magnetic properties of antiferromagnetically coupled CoFeB/Ru/CoFeB, *J. Magn. Magn. Mater.* **290-291**, 1427 (2005).
  - [15] C. Dai and F. Ma, Strong magnon-magnon coupling in synthetic antiferromagnets, *Appl. Phys. Lett.* **118**, 112405 (2021).
  - [16] A. Hubert and R. Schäfer, *Magnetic Domains: The Analysis of Magnetic Microstructures* (Springer, New York, 2008).
  - [17] P. Bruno, Theory of interlayer magnetic coupling, *Phys. Rev. B* **52**, 411 (1995).
  - [18] J. Cho, J. Jung, K.-E. Kim, S.-I. Kim, S.-Y. Park, M.-H. Jung, and C.-Y. You, Effects of sputtering Ar gas pressure in the exchange stiffness constant of  $\text{Co}_{40}\text{Fe}_{40}\text{B}_{20}$  thin films, *J. Magn. Magn. Mater.* **339**, 36 (2013).

- [19] N. Wiese, T. Dimopoulos, M. Rühlig, J. Wecker, H. Brückl, and G. Reiss, Antiferromagnetically coupled CoFeB/Ru/CoFeB trilayers, *Appl. Phys. Lett.* **85**, 2020 (2004).
- [20] J. Swerts, S. Mertens, T. Lin, S. Couet, Y. Tomczak, K. Sankaran, G. Pourtois, W. Kim, J. Meersschaut, L. Souriau, D. Radisic, S. Van Elshocht, G. Kar, and A. Furnemont, BEOL compatible high tunnel magneto resistance perpendicular magnetic tunnel junctions using a sacrificial Mg layer as CoFeB free layer cap, *Appl. Phys. Lett.* **106**, 262407 (2015).
- [21] A. Hashimoto, S. Saito, D. Kim, H. Takashima, T. Ueno, and M. Takahashi, Fe content dependence of synthetic-antiferromagnetic coupling in subnano-crystalline FeCoB/Ru/FeCoB films, *IEEE Trans. Magn.* **42**, 2342 (2006).
- [22] J.-S. Kim, G. Kim, J. Jung, K. Jung, J. Cho, W.-Y. Kim, and C.-Y. You, Control of crystallization and magnetic properties of CoFeB by boron concentration, *Sci. Rep.* **12**, 4549 (2022).
- [23] C. Bilzer, T. Devolder, P. Crozat, C. Chappert, S. Cardoso, and P. P. Freitas, Vector network analyzer ferromagnetic resonance of thin films on coplanar waveguides: Comparison of different evaluation methods, *J. Appl. Phys.* **101**, 074505 (2007).
- [24] T. Devolder and K. Ito, Spin torque switching and scaling in synthetic antiferromagnet free layers with in-plane magnetization, *J. Appl. Phys.* **111**, 123914 (2012).
- [25] R. L. Stamps, Spin configurations and spin-wave excitations in exchange-coupled bilayers, *Phys. Rev. B* **49**, 339 (1994).
- [26] M. Bailleul, Shielding of the electromagnetic field of a coplanar waveguide by a metal film: Implications for broadband ferromagnetic resonance measurements, *Appl. Phys. Lett.* **103**, 192405 (2013).
- [27] See Supplemental Material at <http://link.aps.org/supplemental/10.1103/PhysRevMaterials.7.044404> for the field dependence of the spin wave frequencies and linewidth for a SAF consisting of two layers, each of thickness  $t_{\text{mag}} = 17$  nm. It also displays the spin wave mode profiles for a thick SAF.
- [28] T. Devolder, S.-M. Ngom, A. Mouhoub, J. Letang, J.-V. Kim, P. Crozat, J.-P. Adam, A. Solignac, and C. Chappert, Measuring a population of spin waves from the electrical noise of an inductively coupled antenna, *Phys. Rev. B* **105**, 214404 (2022).
- [29] A. Vansteenkiste, J. Leliaert, M. Dvornik, M. Helsen, F. Garcia-Sanchez, and B. Van Waeyenberge, The design and verification of MuMax3, *AIP Adv.* **4**, 107133 (2014).
- [30] C. Bayer, J. Jorzick, B. Hillebrands, S. O. Demokritov, R. Kouba, R. Bozinoski, A. N. Slavin, K. Y. Guslienko, D. V. Berkov, N. L. Gorn, and M. P. Kostylev, Spin-wave excitations in finite rectangular elements of  $\text{Ni}_{80}\text{Fe}_{20}$ , *Phys. Rev. B* **72**, 064427 (2005).
- [31] H. J. Waring, Y. Li, N. A. B. Johansson, C. Moutafis, I. J. Vera-Marun, and T. Thomson, Exchange stiffness constant determination using multiple-mode FMR perpendicular standing spin waves, *J. Appl. Phys.* **133**, 063901 (2023).
- [32] C. Eyrych, A. Zamani, W. Huttema, M. Arora, D. Harrison, F. Rashidi, D. Broun, B. Heinrich, O. Mryasov, M. Ahlberg, O. Karis, P. E. Jonsson, M. From, X. Zhu, and E. Girt, Effects of substitution on the exchange stiffness and magnetization of Co films, *Phys. Rev. B* **90**, 235408 (2014).
- [33] J. Cho, J. Jung, S.-Y. Cho, and C.-Y. You, Effect of annealing temperature on exchange stiffness of CoFeB thin films, *J. Magn. Magn. Mater.* **395**, 18 (2015).
- [34] G.-M. Choi, Exchange stiffness and damping constants of spin waves in CoFeB films, *J. Magn. Magn. Mater.* **516**, 167335 (2020).
- [35] J. F. Cochran, Light scattering from ultrathin magnetic layers and bilayers, in *Ultrathin Magnetic Structures II: Measurement Techniques and Novel Magnetic Properties*, edited by B. Heinrich and J. A. C. Bland (Springer, New York, 1994), p. 222.
- [36] T. Devolder, T. Tahmasebi, S. Eimer, T. Hauet, and S. Andrieu, Compositional dependence of the magnetic properties of epitaxial FeV/MgO thin films, *Appl. Phys. Lett.* **103**, 242410 (2013).
- [37] B. Hillebrands and G. Güntherodt, Brillouin light scattering in magnetic superlattices, in *Ultrathin Magnetic Structures II: Measurement Techniques and Novel Magnetic Properties*, edited by B. Heinrich and J. A. C. Bland (Springer, New York, 1994), p. 258.
- [38] Y. Chen, X. Fan, Y. Zhou, Y. Xie, J. Wu, T. Wang, S. T. Chui, and J. Q. Xiao, Designing and tuning magnetic resonance with exchange interaction, *Adv. Mater.* **27**, 1351 (2015).
- [39] C. Bilzer, T. Devolder, J.-V. Kim, G. Counil, C. Chappert, S. Cardoso, and P. P. Freitas, Study of the dynamic magnetic properties of soft CoFeB films, *J. Appl. Phys.* **100**, 053903 (2006).
- [40] H. J. Waring, N. A. B. Johansson, I. J. Vera-Marun, and T. Thomson, Zero-field Optic Mode Beyond 20 GHz in a Synthetic Antiferromagnet, *Phys. Rev. Appl.* **13**, 034035 (2020).
- [41] T. Devolder, J.-V. Kim, F. Garcia-Sanchez, J. Swerts, W. Kim, S. Couet, G. Kar, and A. Furnemont, Time-resolved spin-torque switching in MgO-based perpendicularly magnetized tunnel junctions, *Phys. Rev. B* **93**, 024420 (2016).
- [42] T. McKinnon, B. Heinrich, and E. Girt, Spacer layer thickness and temperature dependence of interlayer exchange coupling in Co/Ru/Co trilayer structures, *Phys. Rev. B* **104**, 024422 (2021).